

A single-molecule van der Waals compass

<https://doi.org/10.1038/s41586-021-03429-y>

Received: 16 December 2018

Accepted: 8 March 2021

Published online: 21 April 2021

 Check for updates

Boyan Shen¹, Xiao Chen¹✉, Huiqiu Wang¹, Hao Xiong¹, Eric G. T. Bosch², Ivan Lazić², Dali Cai¹, Weizhong Qian¹, Shifeng Jin³, Xin Liu^{4,5}, Yu Han^{5,6} & Fei Wei¹✉

Single-molecule imaging is challenging but highly beneficial for investigating intermolecular interactions at the molecular level^{1–6}. Van der Waals interactions at the sub-nanometre scale strongly influence various molecular behaviours under confinement conditions^{7–11}. Inspired by the traditional compass¹², here we use a *para*-xylene molecule as a rotating pointer to detect the host–guest van der Waals interactions in the straight channel of the MFI-type zeolite framework. We use integrated differential phase contrast scanning transmission electron microscopy^{13–15} to achieve real-space imaging of a single *para*-xylene molecule in each channel. A good correlation between the orientation of the single-molecule pointer and the atomic structure of the channel is established by combining the results of calculations and imaging studies. The orientations of *para*-xylene help us to identify changes in the van der Waals interactions, which are related to the channel geometry in both spatial and temporal dimensions. This work not only provides a visible and sensitive means to investigate host–guest van der Waals interactions in porous materials at the molecular level, but also encourages the further study of other single-molecule behaviours using electron microscopy techniques.

The compass has played an important part in the process of human development and exploration¹². In a standard compass, a magnetized pointer orients itself roughly north–south to align with the geomagnetic field, in what may have been the earliest principle used to measure the distribution of an electromagnetic field. In recent decades, it has remained a challenge to detect smaller-scale interactions between atoms and molecules under the guidance of such classical principles. Van der Waals interactions between neutral and polarizable atoms, molecules or particles are ubiquitous in various physical, chemical and biological processes across different scales^{16,17}. However, the direct measurements of these forces usually involves various sophisticated nanoscale techniques^{18–20} that are difficult to extend to the study of complex, multi-atom systems. For example, the host–guest van der Waals interactions in nanoscale channels will determine various physical and chemical behaviours of molecules confined within them—such as adsorption, transport, catalysis and phase transition^{7–11}—but it is difficult to investigate these interactions at the single-molecule level using current methods. Analogous to the principle of the traditional compass, here we introduce a rotating molecular pointer into nanoscale channels, in which the positions of the atoms of channels define the direction markers. Precisely identifying the orientations of these pointer molecules can then help to reveal the van der Waals force field formed by the surrounding atoms.

Direct observations of molecular configurations help to better understand interactions at the atomic scale^{1–6}. To identify the exact orientations of the pointer molecules, and therefore to detect the van der Waals interactions, real-space imaging of the pointers and the channel structures is necessary. Advanced imaging techniques

are required in order to really ‘see’ single molecules, especially small organic molecules, owing to their instability and their sensitivity to the electron beam. An imaging mode known as integrated differential phase contrast scanning transmission electron microscopy (iDPC-STEM)^{13–15}—in which light and heavy elements can be imaged together in various beam-sensitive materials^{21–25}—has recently emerged as a possible tool with which to image and investigate single-molecule behaviours in real space. In this work, we establish a nanoscale van der Waals compass in which a single *para*-xylene (PX) molecule—as a rotating pointer—is confined in the straight channels of quasi-two-dimensional (2D) ZSM-5 (MFI-type) zeolite frameworks²⁶. Using iDPC-STEM imaging, we can clearly resolve the atomic structures of the ZSM-5 framework and the orientations of the PX molecules. According to these orientations we can then directly identify the host–guest van der Waals interactions, which are related to the channel geometry in both the spatial and the temporal dimensions.

The MFI-type framework, found for example in the zeolite ZSM-5, consists of a cross-linked channel system formed of straight and sinusoidal channels, which can be imaged from the [010] and [100] directions, respectively (Extended Data Fig. 1). Inspired by the reconstruction of a traditional compass (Fig. 1a), we used single PX molecules as rotating pointers and the Si and O positions in the $\text{Si}_{10}/\text{O}_{10}$ ring of the straight channel of the MFI-type framework as direction markers in order to construct our van der Waals compass (Fig. 1b, c). The elliptical $\text{Si}_{10}/\text{O}_{10}$ ring is numbered to indicate 20 discrete directions that are around 18° apart. Such a straight channel (with a size of $5.6 \times 5.3 \text{ \AA}$) can contain only one C_6 -ring (with a kinetic diameter of around 5.8 \AA) as a size-matched pointer. From previous adsorption studies using MFI-type zeolites^{27–33},

¹Beijing Key Laboratory of Green Chemical Reaction Engineering and Technology, Department of Chemical Engineering, Tsinghua University, Beijing, China. ²Materials and Structural Analysis, Thermo Fisher Scientific, Eindhoven, The Netherlands. ³Research and Development Center for Functional Crystals, Beijing National Laboratory for Condensed Matter Physics, Institute of Physics, Chinese Academy of Sciences, Beijing, China. ⁴School of Chemistry, Dalian University of Technology, Dalian, China. ⁵Physical Sciences and Engineering Division, Advanced Membranes and Porous Materials Center, King Abdullah University of Science and Technology, Thuwal, Saudi Arabia. ⁶Multi-scale Porous Materials Center, Institute of Advanced Interdisciplinary Studies, School of Chemistry and Chemical Engineering, Chongqing University, Chongqing, China. ✉e-mail: chenx123@tsinghua.edu.cn; wf-dce@mail.tsinghua.edu.cn

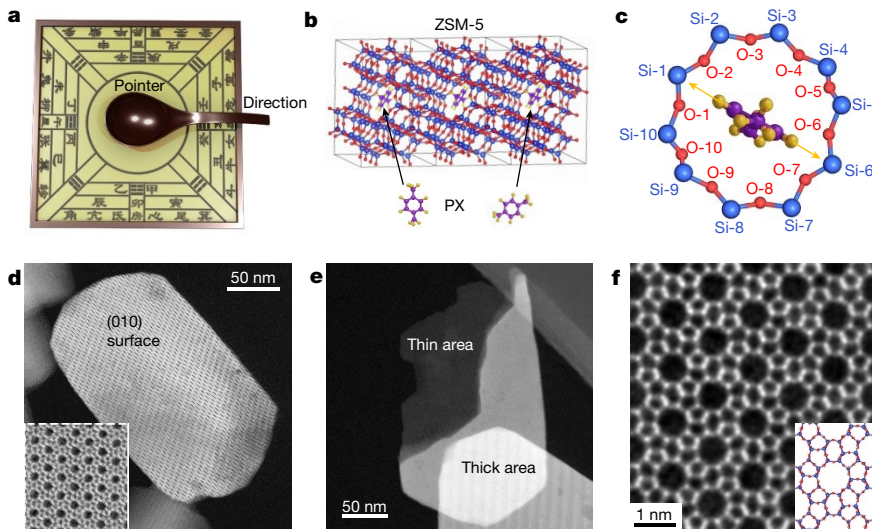


Fig. 1 | Quasi-2D ZSM-5 frameworks for single-molecule van der Waals compass. **a**, Reconstruction of a traditional Chinese compass. **b**, Preparation of a single-molecule van der Waals compass by filling ZSM-5 channels with PX molecules. **c**, Structure of the single-molecule van der Waals compass with a PX pointer molecule in a numbered $\text{Si}_{10}/\text{O}_{10}$ ring. **d**, ADF-STEM image showing the

shape of a short-*b*-axis ZSM-5 crystal. Inset, the straight channels can be imaged from this [010] direction. **e**, ADF-STEM image of an etched ZSM-5 crystal with thin and thick areas. **f**, Atomic-resolution iDPC-STEM image and structural model (inset) of the empty ZSM-5 crystal from the [010] direction.

it is known that monocyclic aromatics can be stably confined at the intersections of the straight and the sinusoidal channels, and their long molecular axes are nearly parallel to the straight channel (along the *b*-axis of the ZSM-5 crystal). The pointer has an energetically preferred orientation due to van der Waals interactions with surrounding Si and O atoms, and it will rotate—as does the pointer in a traditional compass—with the change of channel geometry to enable the detection of the different van der Waals force fields inside the channels.

The quasi-2D ZSM-5 crystals that we used in this work were derived from short-*b*-axis ZSM-5 crystals²⁵ (Extended Data Fig. 2). The annular dark-field (ADF) STEM image (Fig. 1d) shows the shape of the short-*b*-axis ZSM-5 crystals and their smooth (010) surface. After etching with basic reagents (Na_2CO_3 or NaOH), the ZSM-5 crystal becomes hollow with a very thin (quasi-2D) area (Fig. 1e). In this thin area, the channel structures of ZSM-5 can be atomically resolved using iDPC-STEM. The projected positions of Si atoms and empty straight channels can be clearly seen from the [010] direction (Fig. 1f), and are highly consistent with the structural model (inset).

Figure 2a shows a typical etched ZSM-5 crystal that was used for further imaging of the adsorbed PX molecules. The thickness of the thin area in this crystal can be measured by the position-averaged convergent beam electron diffraction (PACBED)

pattern³⁴. Figure 2b shows an experimental PACBED pattern acquired in the thin area, and two simulated PACBED patterns with sample thicknesses of 4 nm and 6 nm. From a more detailed comparison in Extended Data Fig. 3, we confirmed that the thickness of this thin area is between 4 nm and 6 nm (2–3 unit cells of ZSM-5). This was also confirmed by other methods (Extended Data Fig. 4), as well as by matching the zeolite contrast in the iDPC-STEM image to that in simulated results²¹.

Next, PX molecules were adsorbed into the straight channels of this thin area directly from the liquid phase. Figure 2c shows the iDPC-STEM image acquired from the red-framed region of Fig. 2a, and Fig. 2d shows the corresponding intensity profile acquired from the red-framed region in Fig. 2c. After the adsorption of PX, spindle-shaped spots could be clearly observed in some channels—different from the image of the empty ZSM-5 in Fig. 1f. These spots show clear orientations that could be directly identified in the iDPC-STEM image (Fig. 2c). The profile analysis in Fig. 2d also confirmed the presence of PX molecules in the ZSM-5 straight channels. The red line shows the normalized profile of the ZSM-5 into which PX molecules were adsorbed, and the black dashed line shows the normalized profile of empty ZSM-5 along the same direction. The adsorption of PX molecules can be confirmed by the small peaks in the profile valleys of empty channels. As indicated by arrows in Fig. 2d, four channels contain adsorbed

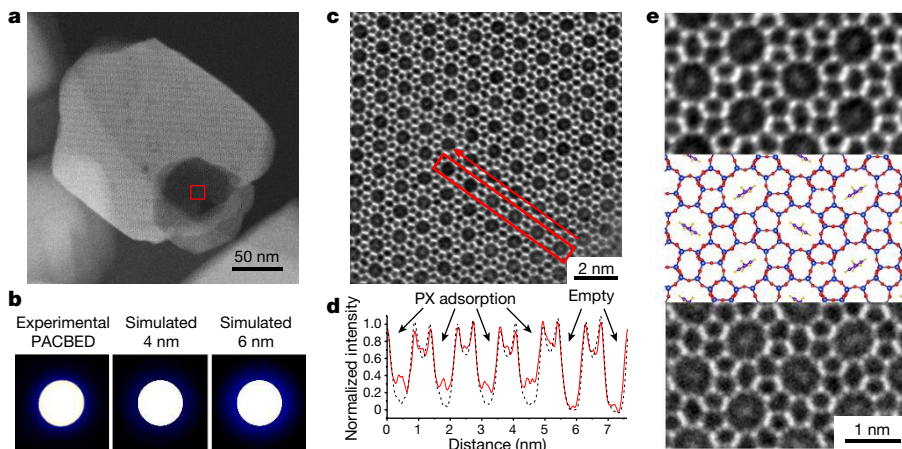


Fig. 2 | Imaging single PX molecules in the straight channels of ZSM-5. **a**, ADF-STEM image of an etched ZSM-5 crystal for imaging PX molecules. **b**, Experimental and simulated PACBED patterns for measuring the thickness of the sample. **c**, **d**, iDPC-STEM image (c) and profile analysis (d) of the thin area of the ZSM-5 crystal (marked by the red box in a). In the intensity profiles, the red line is the normalized intensity profile of the thin area in ZSM-5 filled by PX molecules (marked by the red box in c), whereas the black dashed line is that of empty ZSM-5 channels from the same direction. **e**, Comparison between the magnified iDPC-STEM image (top), the structural model (middle) and the simulated image (bottom) of a single PX molecule in each ZSM-5 channel with a thickness of two unit cells.

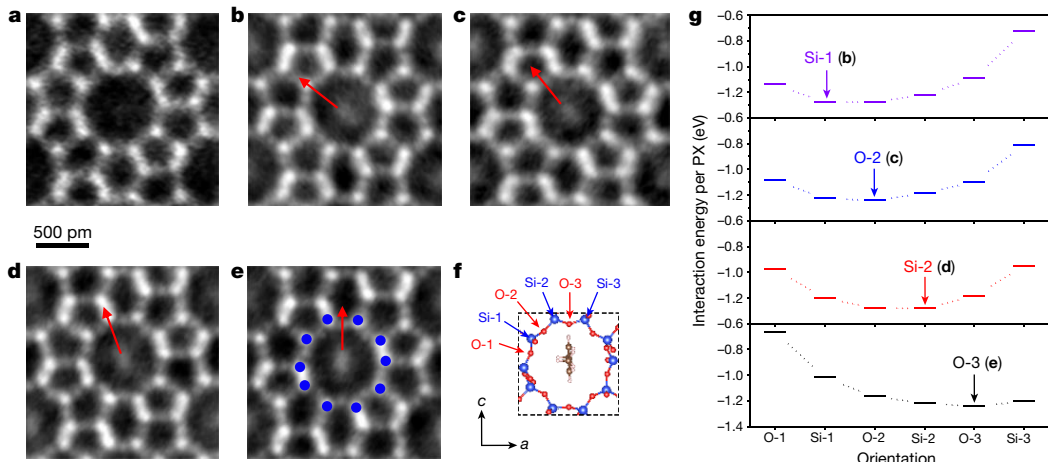


Fig. 3 | Identifying different orientations of PX pointer molecules.

a, Magnified iDPC-STEM image of an empty straight channel. b–e, Magnified iDPC-STEM images of straight channels filled by PX molecules in four different orientations. The red arrows indicate the PX oriented towards Si-1 (b), O-2 (c), Si-2 (d) and O-3 (e) atoms. In e, the blue dots mark the ten projected positions of

Si atoms around the channel. f, Optimized channel geometry and PX configuration calculated according to the projected Si atom positions measured in e. g, Calculated interaction energies of the PX molecules in different orientations in the four channels shown in b–e. The channel models were optimized according to the imaged channel structures.

PX molecules whereas the other two are empty; in these channels, the PX molecules may have been desorbed during sample processing.

The spindle-shaped spots and the orientations of the PX molecules can be seen more clearly in the magnified image in Fig. 2e. Simulated iDPC-STEM images from the [010] direction of ZMS-5 are also shown in Fig. 2e and Extended Data Fig. 5. The agreement between the experimental and the simulated results indicates that the C₆-rings in the PX molecules have specific orientations, as expected in this van der Waals compass. Analysis of the profiles of the experimental and simulated images (Extended Data Fig. 5b) shows that the contrast observed between the PX molecules and the Si atoms is related to the ratio between the number of PX molecules and the number of ZSM-5 unit cells. All ten experimental profiles in Extended Data Fig. 5b indicate that there is only one PX molecule within a sample thickness of between 4 nm and 6 nm. These results provide additional confirmation that the thickness of this etched ZSM-5 crystal was reduced

to 2–3 unit cells, and that it is possible to image a single PX molecule in each channel.

We further investigated the different orientations of PX induced by the host–guest interactions from the magnified iDPC-STEM images of individual channels. Figure 3a shows the iDPC-STEM image of an empty ZSM-5 channel. After PX adsorption there is a spindle-shaped spot in the dark channel, which corresponds to a vertical PX molecule (Fig. 3b–e). The red arrows indicate the orientations of these PX molecules, which are pointing to the Si-1, O-2, Si-2 and O-3 directions (as defined in Fig. 1c). On the basis of the imaging results, we can reveal the correlation between the channel geometry and the orientation of the PX molecule. For example, in Fig. 3e, we mark the ten projected positions of Si atoms around the channel using blue dots. We used the intensity profiles to measure the projected distances to the opposite Si atoms (as shown in Extended Data Fig. 6 and Extended Data Table 1). We then fixed the projected positions of the Si atoms and determined

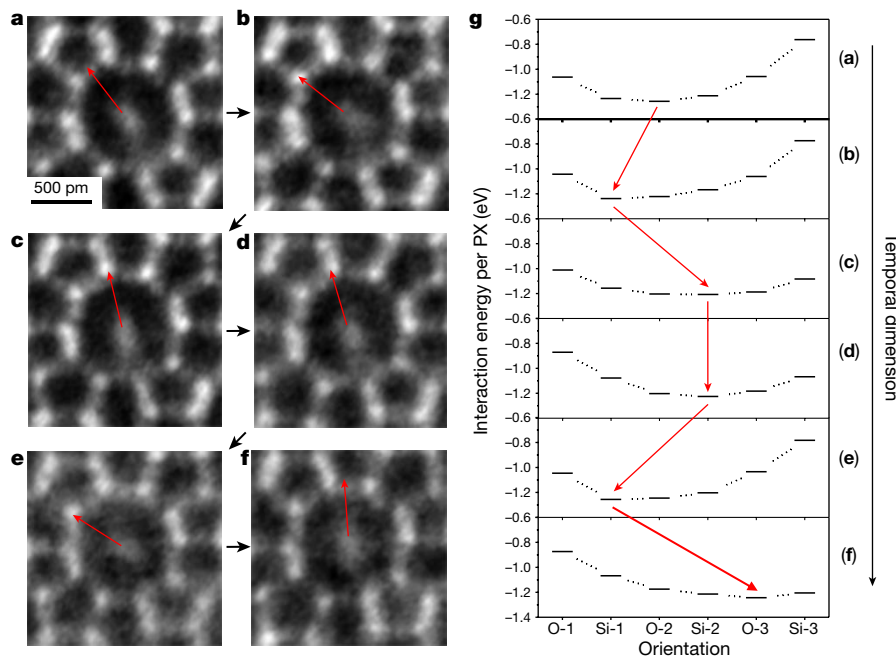


Fig. 4 | Real-time detection of the change in PX orientation with the change in channel geometry.

a–f, Magnified iDPC-STEM images captured continuously from the same channel. The red arrows show the real-time change of PX orientation in this channel. g, Calculated interaction energies of the PX molecules in different orientations in this channel with changing channel geometry. Six channel models are optimized according to the imaged structures in a–f. Orientation changes (marked by arrows) are to those orientations that have the lowest calculated interaction energy for each channel geometry, and correspond well with the observed orientations in each iDPC-STEM image.

the energetically preferred PX configuration in this unit cell using first-principles calculations. Figure 3f shows the PX configuration with the lowest interaction energy in the channel imaged in Fig. 3e. As shown in Extended Data Fig. 6, all calculated PX configurations match well with those in the corresponding experimental images.

For these four channels imaged in Fig. 3b–e, we calculated the host-guest interaction energies when the PX molecule points to the O-1, Si-1, O-2, Si-2, O-3 and Si-3 atoms. The results are summarized in Fig. 3g, in which the orientation observed in the images was found to be that with the lowest interaction energy, as expected. Studying the orientation of PX molecules in additional channels, we find that the ratio of the Si1–Si6 and Si3–Si8 distances seems to be a characteristic parameter to describe the channel geometry, and can be used to demonstrate the correlation between channel geometry and PX orientation more concisely. The results in Extended Data Fig. 7 show that the channels tend to be elongated in the PX-preferred direction, because the van der Waals interaction is sensitive to the distance between interacting objects. Therefore, we conclude that the oriented PX pointer molecule can provide a visual display of the vander Waals force field formed by the surrounding atoms, and the diversity of PX orientations is closely related to the aperiodicity of ZSM-5, which leads to different host–guest van der Waals interactions in different channels.

The above analysis, based on one iDPC-STEM image, reveals the spatial distribution of the PX orientations in channels on the 2D [010] projection. Next, we continuously took several images of the same area to study the change of PX orientation over time. From these images, we were able to capture the change in orientation of one PX molecule in a single channel (Fig. 4a–f, Extended Data Fig. 8) over a time interval of about one minute. The rotation of the PX pointer molecule results from the shift of its equilibrium configuration, which is related to the change of channel geometry (Extended Data Table 2). Persistent irradiation by the electron beam during imaging could induce deformation of the zeolite framework as a result of locally accumulated charging and heating³⁵. In Fig. 4g, we also calculated the interaction energies of PX molecules with different orientations in the channels (channel structures were extracted from Fig. 4a–f). We found a good correspondence between the orientations observed experimentally in the iDPC-STEM images and those that have the lowest calculated interaction energy (Fig. 4g, Extended Data Fig. 9). The results agree with the correlation between the channel geometry and PX orientation that we derived in Fig. 3. Imaging the change in PX orientation demonstrates that the real-time change of channel geometry, and the corresponding change of van der Waals interactions inside the channel, can be detected using this compass strategy.

In summary, a PX molecule in a straight channel of an MFI-type zeolite acts as a single-molecule pointer in a van der Waals compass, which can be directly resolved using iDPC-STEM imaging. In particular, the configuration of the PX molecule can be used to determine host–guest van der Waals interactions in ZSM-5 frameworks. The orientations of the PX pointer molecules provide both the spatial distribution and the real-time change of van der Waals interactions in channels. In addition, single-molecule imaging remains a milestone in nanotechnology and molecular science, especially for small organic molecules confined in porous materials. Other small organic molecules—such as homologues of aromatic molecules—could also be confined and imaged in MFI-type zeolites and other size-matched porous frameworks. As such, this work might provide a general method through which to investigate host–guest interactions in a series of organic–inorganic systems by direct imaging. Such materials have attracted interest in the fields of sorption and catalysis—processes that are difficult to study at the molecular level. Advances in imaging techniques will promote further study of the physical and chemical properties of guest molecules, and bring new insights into the diverse behaviour of single molecules.

Online content

Any methods, additional references, Nature Research reporting summaries, source data, extended data, supplementary information,

acknowledgements, peer review information; details of author contributions and competing interests; and statements of data and code availability are available at <https://doi.org/10.1038/s41586-021-03429-y>.

- Lee, H. J. & Ho, W. Single-bond formation and characterization with a scanning tunneling microscope. *Science* **286**, 1719–1722 (1999).
- Lantz, M. A. et al. Quantitative measurement of short-range chemical bonding forces. *Science* **291**, 2580–2583 (2001).
- Gross, L., Mohn, F., Moll, N., Liljeroth, P. & Meyer, G. The chemical structure of a molecule resolved by atomic force microscopy. *Science* **325**, 1110–1114 (2009).
- Albers, B. J. et al. Three-dimensional imaging of short-range chemical forces with picometre resolution. *Nat. Nanotechnol.* **4**, 307–310 (2009).
- Gross, L. et al. Organic structure determination using atomic-resolution scanning probe microscopy. *Nat. Chem.* **2**, 821–825 (2010).
- Zhang, J. et al. Real-space identification of intermolecular bonding with atomic force microscopy. *Science* **342**, 611–614 (2013).
- Eddaoudi, M. et al. Systematic design of pore size and functionality in isoreticular MOFs and their application in methane storage. *Science* **295**, 469–472 (2002).
- Lai, Z. et al. Microstructural optimization of a zeolite membrane for organic vapor separation. *Science* **300**, 456–460 (2003).
- Rosi, N. L. et al. Hydrogen storage in microporous metal–organic frameworks. *Science* **300**, 1127–1129 (2003).
- Li, J. R., Kuppler, R. J. & Zhou, H. C. Selective gas adsorption and separation in metal–organic frameworks. *Chem. Soc. Rev.* **38**, 1477–1504 (2009).
- Bereciartua, P. J. et al. Control of zeolite framework flexibility and pore topology for separation of ethane and ethylene. *Science* **358**, 1068–1071 (2017).
- Carlson, J. B. Lodestone compass: Chinese or Olmec primacy? *Science* **189**, 753–760 (1975).
- Lazić, I., Bosch, E. G. T. & Lazar, S. Phase contrast STEM for thin samples: integrated differential phase contrast. *Ultramicroscopy* **160**, 265–280 (2016).
- Lazić, I., Bosch, E. G. T., Lazar, S., Wirix, M. & Yücelen, E. Integrated differential phase contrast (iDPC)—direct phase imaging in STEM for thin samples. *Microsc. Microanal.* **22**, 36–37 (2016).
- Lazić, I. & Bosch, E. G. T. in *Advances in Imaging and Electron Physics* Vol. 199 (ed. Hawkes, P. W.) Ch. 3, 75–184 (Elsevier, 2017).
- Margenau, H. Van der Waals forces. *Rev. Mod. Phys.* **11**, 1–35 (1939).
- Israelachvili, J. N. *Intermolecular and Surface Forces* Ch. 6, 107–129 (Academic, 2011).
- Aradhya, S. V., Frei, M., Hybertsen, M. S. & Venkataraman, L. Van der Waals interactions at metal/organic interfaces at the single-molecule level. *Nat. Mater.* **11**, 872–876 (2012).
- Béguin, L., Vernier, A., Chicireanu, R., Lahaye, T. & Browaeys, A. Direct measurement of the van der Waals interaction between two Rydberg atoms. *Phys. Rev. Lett.* **110**, 263201 (2013).
- Kawai, S. et al. Van der Waals interactions and the limits of isolated atom models at interfaces. *Nat. Commun.* **7**, 11559 (2016).
- Yücelen, E., Lazić, I. & Bosch, E. G. T. Phase contrast scanning transmission electron microscopy imaging of light and heavy atoms at the limit of contrast and resolution. *Sci. Rep.* **8**, 2676 (2018).
- Song, D. et al. Visualization of dopant oxygen atoms in a $\text{Bi}_2\text{Sr}_2\text{CaCu}_2\text{O}_{8+\delta}$ superconductor. *Adv. Funct. Mater.* **29**, 1903843 (2019).
- de Graaf, S., Momand, J., Mitterbauer, C., Lazar, S. & Kooi, B. J. Resolving hydrogen atoms at metal–metal hydride interfaces. *Sci. Adv.* **6**, eaay4312 (2020).
- Shen, B., Chen, X., Shen, K., Xiong, H. & Wei, F. Imaging the node-linker coordination in the bulk and local structures of metal–organic frameworks. *Nat. Commun.* **11**, 2692 (2020).
- Shen, B. et al. Atomic spatial and temporal imaging of local structures and light elements inside zeolite frameworks. *Adv. Mater.* **32**, 1906103 (2020).
- Kokotailo, G. T., Lawton, S. L., Olson, D. H. & Meier, W. M. Structure of synthetic zeolite ZSM-5. *Nature* **272**, 437–438 (1978).
- van Koningsveld, H., Tuinstra, F., Van Bekkum, H. & Jansen, J. C. The location of *p*-xylene in a single crystal of zeolite H-ZSM-5 with a new, sorbate-induced, orthorhombic framework symmetry. *Acta Crystallogr. B* **45**, 423–431 (1989).
- Goyal, R., Fitch, A. N. & Jobic, H. Powder neutron and X-ray diffraction studies of benzene adsorbed in zeolite ZSM-5. *J. Phys. Chem. B* **104**, 2878–2884 (2000).
- Taylor, J. C. Hexadeuteriobenzene locations in the cavities of ZSM-5 zeolite by powder neutron diffraction. *J. Chem. Soc. Chem. Commun.* **15**, 1186–1187 (1987).
- Fyfe, C. A., Lee, J. S. J., Cranswick, L. M. D. & Swainson, I. Powder neutron diffraction determination of the structure of the *o*-xylene/zeolite ZSM-5 complex. *Microporous Mesoporous Mater.* **112**, 299–307 (2008).
- Fyfe, C. A. & Brouwer, D. H. Optimization, standardization, and testing of a new NMR method for the determination of zeolite host–organic guest crystal structures. *J. Am. Chem. Soc.* **128**, 11860–11871 (2006).
- Fyfe, C. A., Diaz, A. C., Grondhey, H., Lewis, A. R. & Förster, H. Solid state NMR method for the determination of 3D zeolite framework/sorbate structures: $^1\text{H}/^{29}\text{Si}$ CP MAS NMR study of the high-loaded form of *p*-xylene in ZSM-5 and determination of the unknown structure of the low-loaded form. *J. Am. Chem. Soc.* **127**, 7543–7558 (2005).
- Boronat, M. & Corma, A. What is measured when measuring acidity in zeolites with probe molecules? *ACS Catal.* **9**, 1539–1548 (2019).
- LeBeau, J. M., Findlay, S. D., Allen, L. J. & Stemmer, S. Position averaged convergent beam electron diffraction: theory and applications. *Ultramicroscopy* **110**, 118–125 (2010).
- Chen, Q. et al. Imaging beam-sensitive materials by electron microscopy. *Adv. Mater.* **32**, 1907619 (2020).

Publisher's note Springer Nature remains neutral with regard to jurisdictional claims in published maps and institutional affiliations.

© The Author(s), under exclusive licence to Springer Nature Limited 2021

Methods

Synthesis of quasi-2D ZSM-5 crystals

The short-*b*-axis ZSM-5 crystal shown in Fig. 1d was synthesized by a hydrothermal method. Tetrapropylammonium hydroxide (TPAOH) was used as the structure-directing agent. The silicon source was tetraethyl orthosilicate (TEOS), and the aluminium source was Al(NO₃)₃·9H₂O. In a typical synthesis, 13.1g TPAOH, 11.2g TEOS, 2.0g urea, 0.3g Al(NO₃)₃·9H₂O, 0.1g NaOH and 0.1g isopropanol (IPA) were added into 18.4g H₂O under stirring. After stirring for 1–2 h at room temperature, the gel was transferred into a Teflon-lined autoclave for temperature-programming crystallization. The crystallization temperature was increased from room temperature to 180 °C at a rate of 15 °C h⁻¹, and then held constant for 48 h. Subsequently, the crystallization was quenched with cold water. The product was filtered, washed, dried at 110 °C in air and then calcined at 550 °C for 5 h to remove the remaining organic template.

The quasi-2D ZSM-5 areas shown in Fig. 1e can be obtained using two etching methods, based on modification of the above synthetic process. In the first method, we transferred the above short-*b*-axis ZSM-5 crystals into 1 M Na₂CO₃ solution at 80 °C for 24 h. The ZSM-5 crystals were etched by Na₂CO₃ to form a hollow shape with quasi-2D areas. In the second method, we directly reduced the amount of Al(NO₃)₃·9H₂O to 0.1g (to give a higher Si/Al ratio). Meanwhile, the heating rate was reduced to 6 °C h⁻¹. The extended crystallization time enables the remaining NaOH to directly etch ZSM-5 crystals just after the crystallization. In both of these two methods, the short-*b*-axis ZSM-5 crystals can be efficiently etched by the basic reagents (Na₂CO₃ or NaOH) to give quasi-2D areas with a uniform thickness of 2–3 unit cells. Before the filling with PX and imaging, the obtained crystals were separated by filtration and washed three times, and subsequently dried at 110 °C in air. Then, the Na-ZSM-5 was converted into H-ZSM-5 by three ion exchanges with 1 M NH₄NO₃ solution and subsequent calcination in air at 550 °C for 5 h.

Filling ZSM-5 with PX molecules

PX molecules were absorbed into the straight channels of ZSM-5 directly from the liquid phase. ZSM-5 powder and pure PX liquid were added into a 1 ml centrifuge tube. The ZSM-5 crystals were dispersed in PX using ultrasound for 30 min to diffuse the PX molecules into the ZSM-5 framework. Before the STEM observations, the specimens were heated at 100–200 °C to remove the PX molecules on or near the surfaces. As such, it is possible to capture a single PX molecule in each channel in the quasi-2D area.

Imaging conditions and simulations

The iDPC-STEM experiments were performed using a Cs-corrected scanning transmission electron microscope (FEI Titan Cubed Themis G2 300) operated at 300 kV. The microscope was equipped with a DCOR+ spherical aberration corrector for the electron probe which was aligned before the experiments using a standard gold sample. The following aberration coefficients were measured as: A₁ = 1.41 nm; A₂ = 11.5 nm; B₂ = 22.2 nm; C₃ = 2.05 μm; A₃ = 525 nm; S₃ = 177 nm; A₄ = 8.81 μm, D₄ = 2.39 μm, B₄ = 13.2 μm, C₅ = -3.95 mm, A₅ = 295 μm, S₅ = 111 μm and R₅ = 102 μm. The convergence semi-angle was 15 mrad, the beam current was lower than 0.5 pA (the measurement was limited by the precision of the Faraday cup), the collection angle was 4–22 mrad, and the dwell time of probe scanning was 32 μs.

The image simulations were conducted on the basis of the multi-slice method³⁶, which can be extended to support iDPC-STEM as explained in previous studies^{13,15,37}. Considering the convergence angle of the beam (15 mrad), the thickness of the sample of 2–3 ZSM-5 unit cells (4–6 nm) and the fact that the sample consists of mostly Si and light elements, this sample can be considered thin³⁸. The parameters for simulations—such as the convergence angle, the collection angle and the applied dose—were selected to be the same as those in our imaging experiments. In the simulations, four images were obtained from four

segments of the four-quadrant detector spanning 4–22 mrad in default orientation. Shot noise was added to these four images according to the experimental data. The resulting noisy quadrant images are blurred with a Gaussian blur to account for incoherency of the source before the final iDPC-STEM images are formed^{13,15,21}.

Measurement of sample thickness

The thickness of the quasi-2D ZSM-5 crystal was measured using the PACBED method. During PACBED acquisition, the beam was scanned continuously over an area of around 2 × 2 unit cells at an acceleration voltage of 300 kV with a convergence semi-angle of 10 mrad. The PACBED patterns were recorded on an BM-Ceta camera (512 × 512 pixels). The recording time for each pattern was 8 s at a beam current of around 1 pA. Then, the theoretical PACBED patterns of ZSM-5 crystals were simulated with a MuSTEM multislice simulation code³⁹, developed at the University of Melbourne. Simulations of the PACBED patterns for different sample thicknesses were performed using the same parameters as we applied in the thickness measurement experiments (including the acceleration voltage and the convergence semi-angle). Quantitatively, the least-squares fitting was carried out on the PACBED patterns from the thin area and the simulations⁴⁰ (Extended Data Fig. 3), showing that the thickness of this thin area was between 4 and 6 nm.

First-principles energy calculations

All periodic first-principles calculations were carried out using the Perdew–Burke–Ernzerhof exchange-correlation functional in the generalized gradient approach, as implemented in the Vienna ab initio simulation package^{41,42}. The projected augmented wave formalism was used to consider the effect of the core and valence electrons in the valence density⁴³, and the valence electrons were described by plane wave basis sets with a cut-off energy of 400 eV. Gamma points were used for Brillouin zone integration. The van der Waals dispersion interaction between the PX and the zeolite was considered using the DFT-D3 scheme^{44,45}. The energy and force convergence criteria were 1.0×10^{-5} eV and $0.03 \text{ eV } \text{\AA}^{-1}$, respectively, in all calculations. The single unit cell ($a = 20.02$, $b = 19.90$ and $c = 13.38 \text{ \AA}$) containing 96 Si atoms and 192 O atoms was used to represent the MFI lattice.

The channel geometry was then optimized on the basis of imaging results. The projected distances between the opposite Si atoms in the channels in Figs. 3 and 4 are summarized in Extended Data Table 1 and 2, respectively. We modified the projected distances between these opposite Si atoms to match those measured in the imaging results, and then fixed them during further optimization. We placed a PX molecule at the intersection of the straight and sinusoidal channels. The PX configuration and the MFI framework structure were fully optimized in terms of all atoms except the fixed Si atoms. Until the forces were smaller than $0.03 \text{ eV } \text{\AA}^{-1}$, the total energy of the optimized MFI framework with a confined PX molecule (with the most probable configuration in Extended Data Fig. 6) was calculated. After this threshold was reached, other sub-optimal PX orientations in these channels were obtained by rotating the PX molecule along the *b*-axis of the MFI framework. MFI frameworks with different sub-optimal PX orientations were used to perform single-point energy calculations. The interaction energy of the PX molecule in the MFI channel (E_{in}) is defined as the energy difference between the total energy, PX + ZSM-5, ($E_{\text{PX+ZSM-5}}$) and the sum of the energies of free PX (E_{PX}) and empty ZSM-5 ($E_{\text{ZSM-5}}$) (obtained by the same method). It can therefore be calculated as $E_{\text{in}} = E_{\text{PX+ZSM-5}} - E_{\text{PX}} - E_{\text{ZSM-5}}$. The lowest interaction energy obtained is about -1.2 eV for each PX molecule, which roughly agrees with the previous calculated and experimental results for aromatic molecules.

Data availability

The data supporting the findings of this study are available from the corresponding authors upon request.

Article

36. Kirkland, E. J. *Advanced Computing in Electron Microscopy* 3rd edn (Springer, 2020).
37. Bosch, E. G. T. & Lazić, I. Analysis of HR-STEM theory for thin specimen. *Ultramicroscopy* **156**, 59–72 (2015).
38. Bosch, E. G. T. & Lazić, I. Analysis of depth-sectioning STEM for thick samples and 3D imaging. *Ultramicroscopy* **207**, 112831 (2019).
39. Allen, L. J., D'Alfonso, A. J. & Findlay, S. D. Modelling the inelastic scattering of fast electrons. *Ultramicroscopy* **151**, 11–22 (2015).
40. Gao, W. et al. Real-space charge-density imaging with sub-ångström resolution by four-dimensional electron microscopy. *Nature* **575**, 480–484 (2019).
41. Perdew, J. P., Burke, K. & Ernzerhof, M. Generalized gradient approximation made simple. *Phys. Rev. Lett.* **77**, 3865–3868 (1996).
42. Kresse, G. & Furthmüller, J. Efficient iterative schemes for ab initio total-energy calculations using a plane-wave basis set. *Phys. Rev. B* **54**, 11169–11186 (1996).
43. Blöchl, P. E. Projector augmented-wave method. *Phys. Rev. B* **50**, 17953–17979 (1994).
44. Grimme, S. Accurate description of van der Waals complexes by density functional theory including empirical corrections. *J. Comput. Chem.* **25**, 1463–1473 (2004).
45. Grimme, S. Semiempirical GGA-type density functional constructed with a long-range dispersion correction. *J. Comput. Chem.* **27**, 1787–1799 (2006).

Acknowledgements We thank Q. Zhang and W. Gao for discussions. This work was supported by the National Key Research and Development Program of China (2018YFB0604801), the

National Natural Science Foundation of China (21771029, 202013981 and 22005170) and the National Key R&D Program of China (2017YFB0602204). Y.H. thanks the Center Applied Research Fund (FCC/1/1974-16-01) from King Abdullah University of Science and Technology. We thank the Tsinghua National Laboratory for Information Science and Technology for assistance with the energy simulation.

Author contributions B.S., X.C. and F.W. conceived this project and designed the studies; B.S. and X.C. performed the electron microscopy experiments and data analysis; H.W. carried out the energy calculations; H.W. and H.X. prepared the zeolite samples; E.G.T.B. and I.L. performed the simulation of iDPC-STEM images; D.C., W.Q., S.J., X.L. and Y.H. helped with the data analysis; and B.S. and X.C. wrote the manuscript.

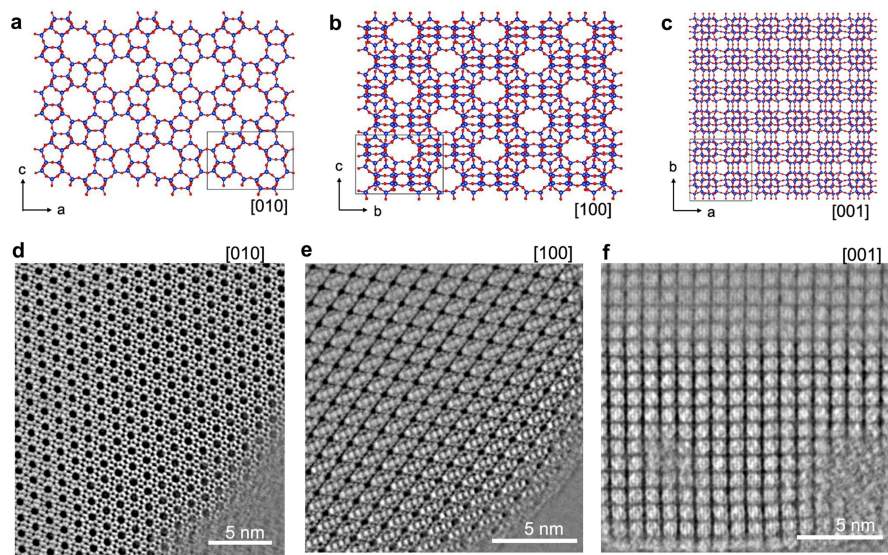
Competing interests The authors declare no competing interests.

Additional information

Correspondence and requests for materials should be addressed to X.C. or F.W.

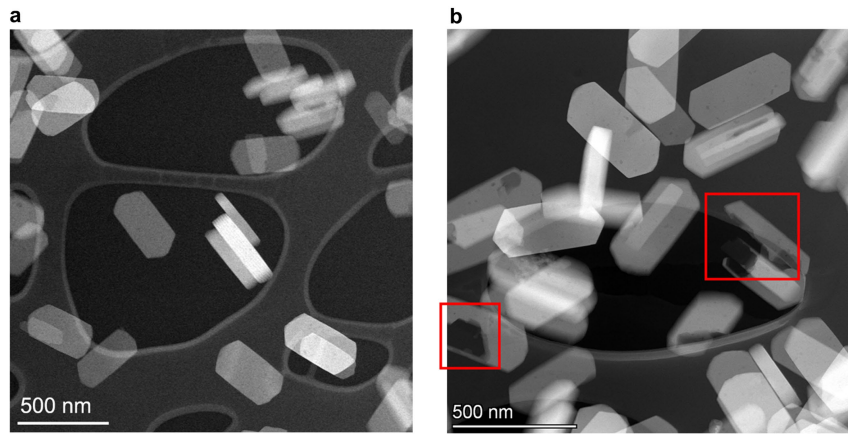
Peer review information *Nature* thanks Bruce Gates, Xiadong Zou and the other, anonymous, reviewer(s) for their contribution to the peer review of this work.

Reprints and permissions information is available at <http://www.nature.com/reprints>.

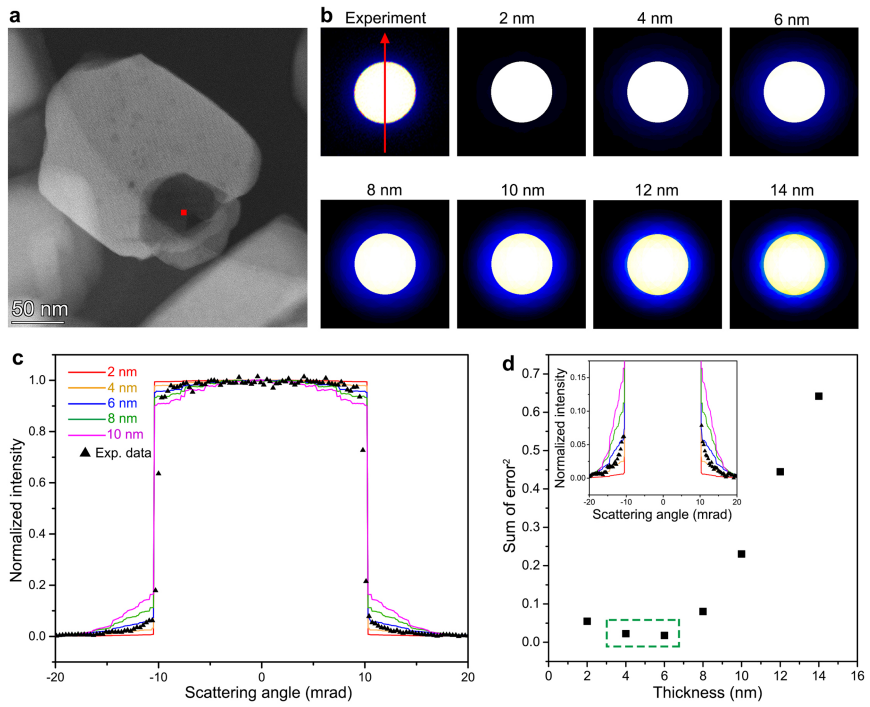


Extended Data Fig. 1 | Atomic structure of MFI-type framework. **a–c**, The structure of the MFI-type framework. **d–f**, iDPC-STEM images of the empty ZSM-5 framework taken along the three main crystallographic axes.

Article

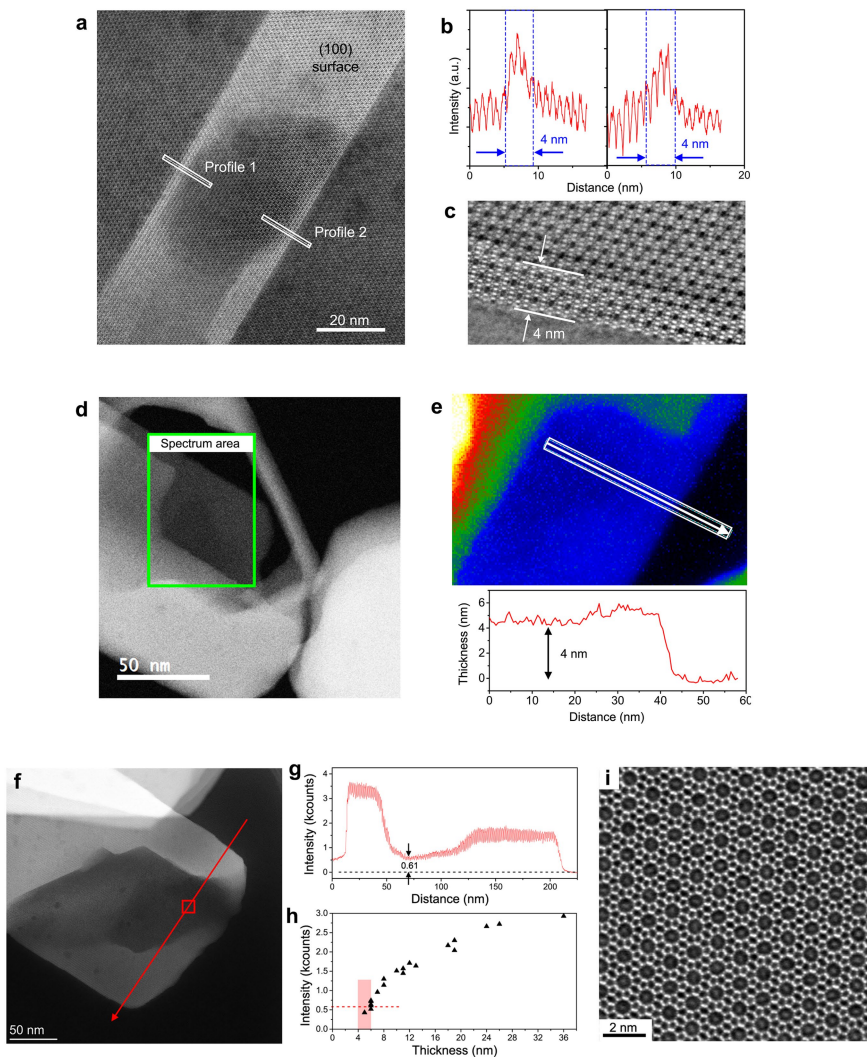


Extended Data Fig. 2 | Shapes of ZSM-5 crystals. **a**, ADF-STEM image showing the shapes of pristine short-*b*-axis ZSM-5 crystals. **b**, ADF-STEM images showing the hollow shapes of etched ZSM-5 crystals (quasi-2D areas are marked with red boxes).



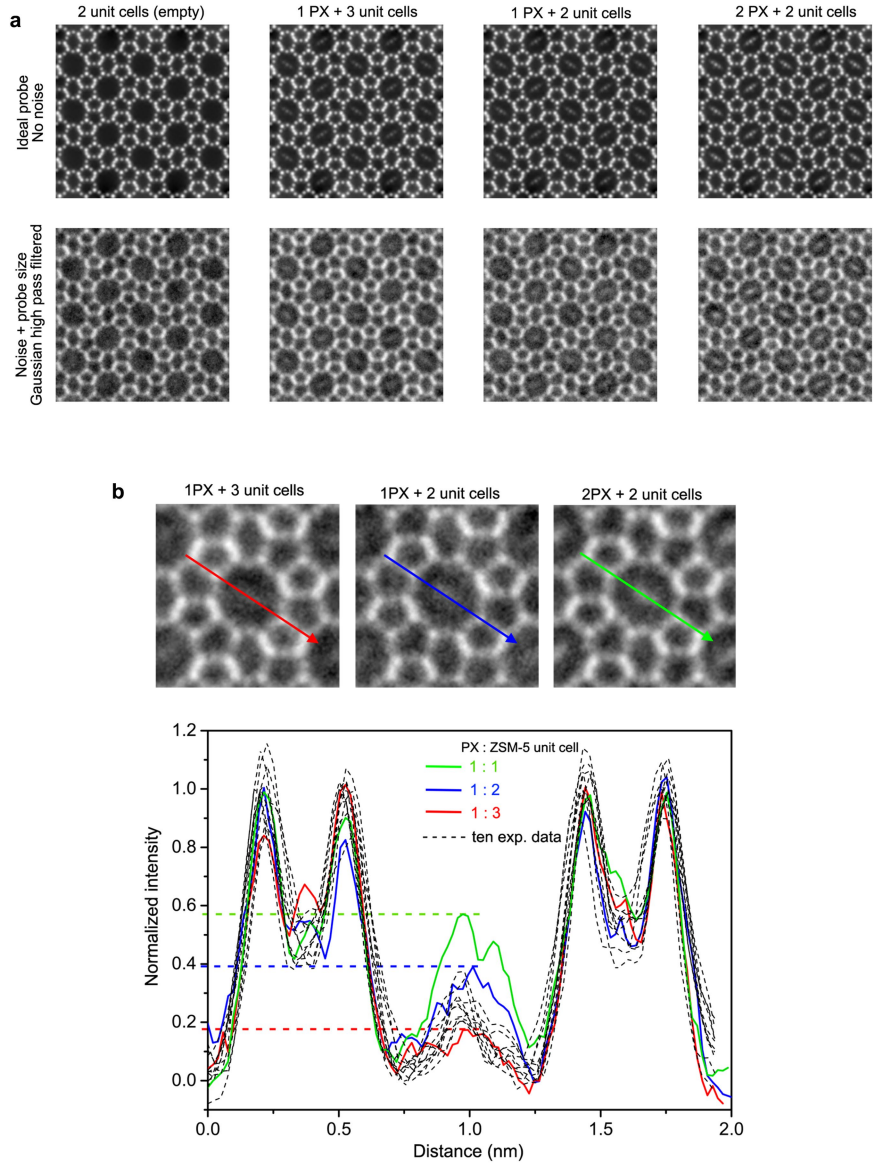
Extended Data Fig. 3 | Measuring sample thickness using the PACBED method. **a**, ADF-STEM image of the same ZSM-5 crystal as in Fig. 2. **b**, Experimental PACBED pattern at the thin area in **a** (marked by the red spot) and simulated PACBED patterns with different sample thicknesses. **c**, Analysis of PACBED patterns by comparing the profiles of experimental and simulated patterns. All profiles are along the same direction, marked by the red arrow in **a**. **d**, Least-squares fitting of the experimental PACBED patterns with the simulated patterns. The inset shows the magnified profiles in **c**. The fitting also indicates that the thickness is most likely to be between 4 nm and 6 nm.

b. The experimental data fall between those of the simulated profiles with thicknesses of 4 nm and 6 nm. **d.** Least-squares fitting of the experimental PACBED patterns with the simulated patterns. The inset shows the magnified profiles in **c**. The fitting also indicates that the thickness is most likely to be between 4 nm and 6 nm.


Extended Data Fig. 4 | Measuring sample thickness using other methods.

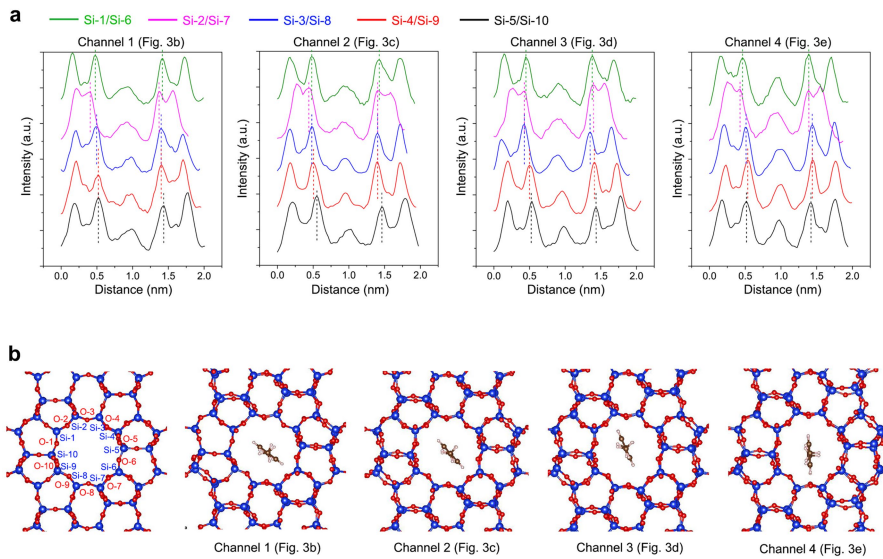
a, ADF-STEM image of an etched ZSM-5 crystal from the lateral view ([100] direction). **b**, Profile analysis of the thin areas from the lateral view. **c**, iDPC-STEM image of the lateral lattice of an etched ZSM-5 crystal, showing a thickness of about 4 nm. **d**, ADF-STEM image of etched ZSM-5 crystals with an obvious thin area. **e**, Thickness mapping and profile analysis obtained by electron energy loss spectroscopy. The measured thickness is about 4 nm. It should be noted that there are uncertainties in these thickness values, mainly due to errors in estimating the mean free path for inelastic scattering.

f, ADF-STEM image of an etched ZSM-5 crystal for PX imaging. **g**, Profile analysis of the etched ZSM-5 crystal in **f**. This profile includes the image intensities relative to the background along the direction marked by the red arrow in **f**. **h**, Relation between ADF-STEM intensity and sample thickness. The intensities are obtained from the intensity profiles of ADF-STEM images, and the thicknesses are measured by the least-squares fitting of PACBED patterns. On the basis of the intensity of the thin area in **g** (around 0.61 kcounts), we can obtain the thickness of this area as 4–6 nm. **i**, iDPC-STEM image of the thin area marked by the red box in **f**. The PX molecules in the channels can be clearly seen.



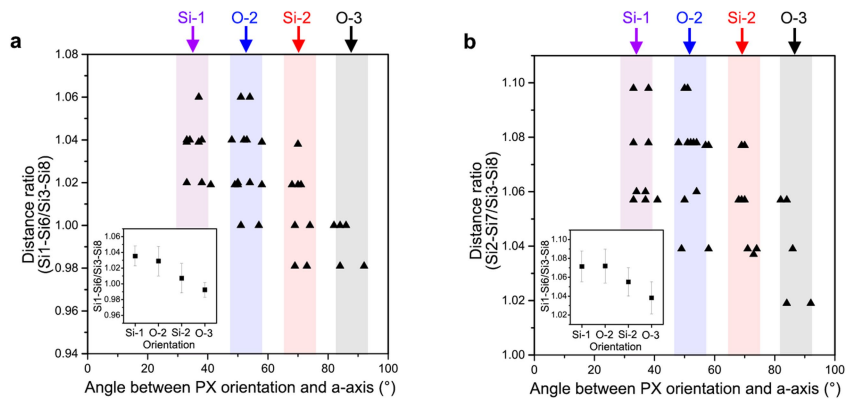
Extended Data Fig. 5 | Simulations of iDPC-STEM imaging. **a**, Simulated iDPC-STEM images with different numbers of PX molecules and ZSM-5 unit cells (that is, different ratios of PX and ZSM-5 thickness). The top four images are the simulated results with an ideal probe and no noise. The bottom four images include the noise, the probe sizes and high-pass filtering based on the experimental conditions. **b**, Profile analysis of the simulated iDPC-STEM images compared with the experimental images. The normalized intensity

profiles of three channels (three coloured arrows shown in the top three images) with different ratios of PX to ZSM-5 thickness indicate that the height of PX peak is related to this ratio of PX to ZSM-5. The heights of 10 PX peaks in 10 channels obtained in Fig. 2c are just between those of 1 PX in 2 unit cells and 1 PX in 3 unit cells. Because the measured thickness of the quasi-2D area is 4–6 nm (2–3 ZSM-5 unit cells), the PX number in each channel can only be one.


Extended Data Fig. 6 | Channel structures and energy calculations.

a, Intensity profiles measuring the projected distances of opposite Si atoms in four channels in Fig. 3. **b**, The most probable configurations of PX molecules in

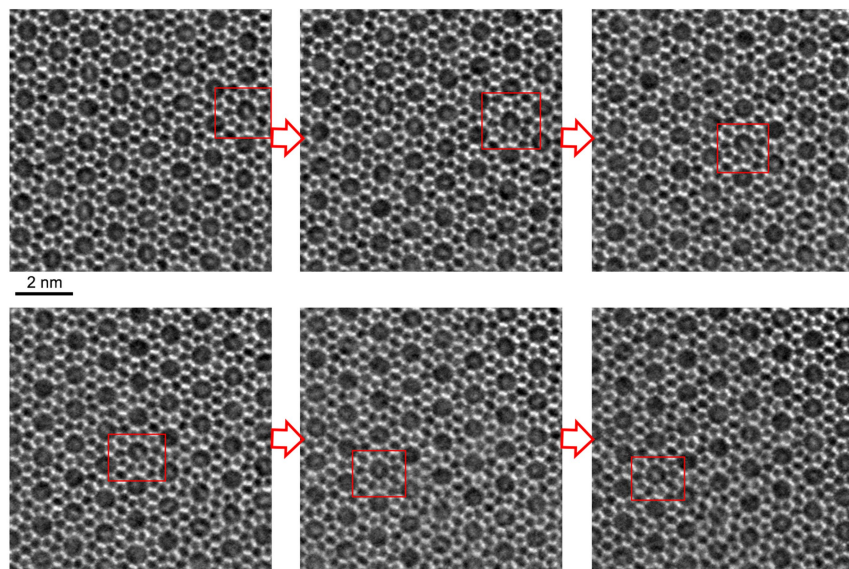
the optimized models of four channels in Fig. 3 based on first-principles calculations.



Extended Data Fig. 7 | Correlation between PX orientation and channel geometry. **a, b,** Distance ratios of $\text{Si}_1\text{-}\text{Si}_6/\text{Si}_3\text{-}\text{Si}_8$ (a) and $\text{Si}_2\text{-}\text{Si}_7/\text{Si}_3\text{-}\text{Si}_8$ (b) and their relation to the angles between the PX orientation and the a axis of the ZSM-5 crystal. The insets give the mean values and the standard deviations

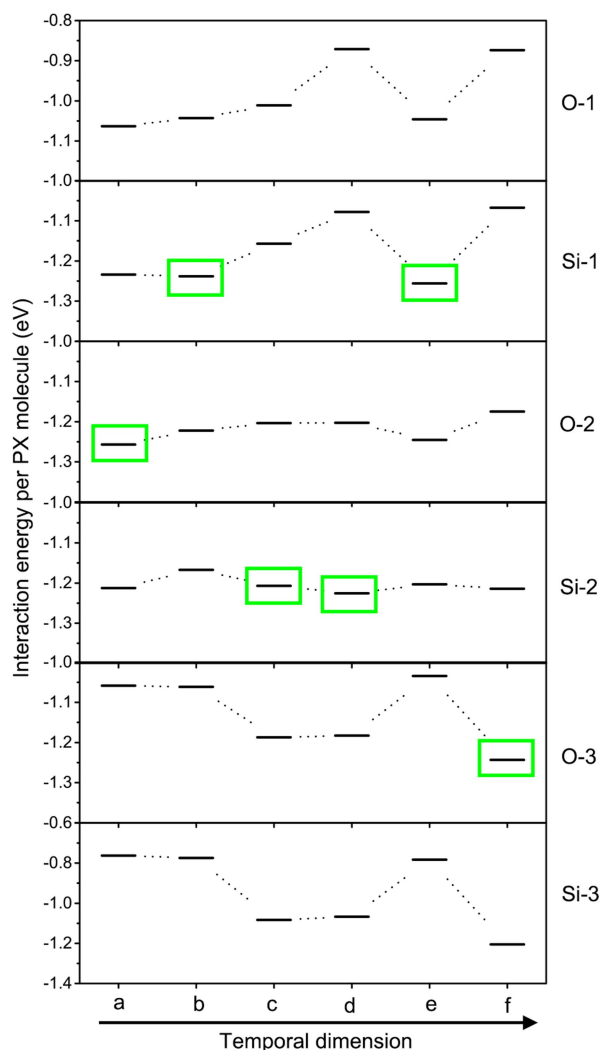
(error bars) of distance ratios when we summarized the data with the same PX orientations together. Both of these ratios show a notable downward trend with increasing orientation angle, which reveals the correlation between PX orientation and channel geometry.

Article



Extended Data Fig. 8 | Real-time change of PX orientation. iDPC-STEM images continuously captured from the same area. The red boxes highlight the same channel in each image—the channel in which we analysed the change of

channel geometry and the rotation of the PX molecule in Fig. 4 (note that there is a small shift in the sample between images).



Extended Data Fig. 9 | Energy calculations with changing channel geometry.

geometry. Time-dependent change of the calculated interaction energy when each PX orientation was fixed and only the channel geometry was changed, as observed in Fig. 4. The green boxes indicate the lowest energy at each time, which is usually the minimum point on the curve of each PX orientation.

Article

Extended Data Table 1 | Projected distances of opposite Si atoms in four images

	Si-1/Si-6 distance (nm)	Si-2/Si-7 distance (nm)	Si-3/Si-8 distance (nm)	Si-4/Si-9 distance (nm)	Si-5/Si-10 distance (nm)
Channel 1 (Fig. 3b)	0.942	0.960	0.906	0.889	0.924
Channel 2 (Fig. 3c)	0.942	0.960	0.924	0.906	0.906
Channel 3 (Fig. 3d)	0.942	0.977	0.924	0.906	0.906
Channel 4 (Fig. 3e)	0.924	0.960	0.942	0.906	0.906

Relates to images in Fig. 3.

Extended Data Table 2 | Projected distances of opposite Si atoms in six images

	Si-1/Si-6 distance (nm)	Si-2/Si-7 distance (nm)	Si-3/Si-8 distance (nm)	Si-4/Si-9 distance (nm)	Si-5/Si-10 distance (nm)
Channel 1 (Fig. 4a)	0.942	0.977	0.906	0.906	0.906
Channel 2 (Fig. 4b)	0.960	0.977	0.924	0.924	0.889
Channel 3 (Fig. 4c)	0.924	0.960	0.924	0.924	0.906
Channel 4 (Fig. 4d)	0.906	0.977	0.924	0.924	0.889
Channel 5 (Fig. 4e)	0.960	0.977	0.924	0.906	0.889
Channel 6 (Fig. 4f)	0.924	0.960	0.942	0.924	0.906

Relates to images in Fig. 4.